catalysts

MDPI

Article

Synthesis and Evaluation of PtNi Electrocatalysts for CO and Methanol Oxidation in Low Temperature Fuel Cells

Griselda Caballero-Manrique [1,2], Julia Garcia-Cardona [1], Enric Brillas [1], Juan A. Jaén [2], John Manuel Sánchez [1,2] and Pere L. Cabot [1,*]

[1] Laboratori d'Electroquímica dels Materials i del Medi Ambient, Secció de Química Física, Facultat de Química, Universitat de Barcelona, Martí i Franquès 1-11, 08028 Barcelona, Spain; griselda.caballero@up.ac.pa (G.C.-M.); jul.gar.95@gmail.com (J.G.-C.); brillas@ub.edu (E.B.); john507sanchez@hotmail.com (J.M.S.)

[2] Department of Physical Chemistry, Universidad de Panamá, Panama 69860076, Panama; juan.jaen@up.ac.pa

* Correspondence: p.cabot@ub.edu; Tel.: +34-93-403-92-36

Received: 27 April 2020; Accepted: 17 May 2020; Published: 19 May 2020

Abstract: Pt(Ni)/C and PtRu(Ni)/C catalysts were synthesized by electroless deposition of Ni on a carbon dispersion followed by sequenced Pt deposition and spontaneous deposition of Ru species. The structural analyses of the catalysts with 88:12 and 98:2 Pt:Ni atomic ratios pointed out to the formation of small hexagonal Ni crystallites covered by thin cubic Pt surface structures with no evidence about PtNi alloy formation. The onset potentials for CO oxidation on Pt(Ni)/C and PtRu(Ni)/C were about 0.10 and 0.24 V more negative than those of Pt/C, thus indicating their better CO tolerance. The surface Ru species appeared to have the major effect by facilitating the CO removal by the bifunctional mechanism. The onset potential for the methanol oxidation reaction (MOR) of Pt(Ni)/C was about 0.15 V lower than that of Pt/C. The mass and specific activities together with the exchange current densities of the Pt(Ni)/C catalysts were also higher than those of Pt/C, making in evidence their higher activity in front of the MOR. The Tafel slopes for the MOR on Pt(Ni)/C suggested different reaction mechanism than on Pt/C. The electronic (ligand) effect of Ni on Pt was considered the main reason to explain the higher activity of Pt(Ni)/C in front of the CO oxidation and the MOR.

Keywords: Pt(Ni)/C catalysts; PtRu(Ni)/C catalysts; galvanic exchange; Ru spontaneous deposition; CO oxidation; methanol oxidation reaction

1. Introduction

The shortage of fossil fuel deposits increases over time along with the energy demand, causing a negative impact on the environment. Thus, many researchers worldwide have turned their attention toward a common goal of developing alternative energy sources. After several decades, fuel cells have emerged as an alternative to other energy sources. There is considerable research on this topic, encompassing the study of aspects such as the production, storage and transportation of hydrogen; new ways of obtaining hydrogen and new catalytic materials, among others [1]. A fuel cell is an electrochemical device that converts directly the chemical energy of a reaction into electrical energy. It allows electricity to be generated by two electrodes, an anode and a cathode, separated by an electrolyte, combining hydrogen and oxygen electrochemically, in the absence of combustion reactions [2]. Very high efficiencies can be reached because they are not affected by Carnot's heat engine limitation and the absence of moving components within the device, reducing the friction losses that are present in an internal combustion engine.

The cleanest fuel is pure hydrogen. However, the cheapest H_2 is still obtained from hydrocarbon reforming and it is well known that it contains a remaining CO, which easily poisons the Pt catalyst generally used in the low temperature fuel cells such as proton exchange membrane fuel cells (PEMFCs). On the other hand, there have been significant efforts in the study of the electrochemical oxidation of alcohols and other hydrocarbons. Organic liquid fuels are characterized by a high energy density, whereas the electromotive force associated with their electrochemical oxidation to CO_2 is comparable to that of hydrogen combustion to produce water [3–5]. The anode reaction for the methanol oxidation reaction (MOR) on Pt and Pt-based alloys in direct-methanol fuel cells (DMFCs) has been explored since many years ago [3,6–9]. DMFCs, which also use proton exchange membranes as electrolyte, are fed directly by a methanol/water mixture at the anode. Methanol is oxidized to CO_2, but by-products such as formaldehyde, formic acid, and especially the intermediate carbon monoxide, which decrease the cell efficiency, are formed. The PtRu alloys are at present the best candidates for the MOR and their good performance are explained by the bifunctional mechanism and the electronic effect of the Ru alloying atom [7–19]. According to the theory of the bifunctional mechanism, the formation of hydroxylated species on Ru at low potentials favor the formation of CO_2 from adsorbed CO on Pt:

In addition, the modification of the electronic structure of Pt by Ru can decrease the adsorption strength of the poisoning species, thus contributing together with the bifunctional mechanism to increase the rate of Equation (1).

$$\text{Pt-CO} + \text{Ru(OH)} \rightarrow \text{Pt} + \text{Ru} + \text{CO}_2 + \text{H}^+ + \text{e}^- \quad (1)$$

The electrooxidation of ethanol is also of special interest because it has a high energy content, with 12 electrons per mol, low toxicity and little environmental concerns [4,5]. The ethanol oxidation reaction (EOR) is more complex than that of methanol because it requires de C-C bond breaking and the CO_2 yield is small in mild conditions of temperature and pressure [20,21]. Good performances have been reported when using PtRu, PtRh, PtPd and PtSn catalysts [20,22–26]. Conversely, Fe, Ni and Co supported on micro/nano-structured carbon did not present catalytic activity for the EOR [27]. The C–C bond breaking was favored with PtRh. However, the ethanol conversion to CO_2 is still limited.

At present, the benchmark catalysts for PEMFCs in the industrial-related applications are carbon-supported Pt and Pt-based alloys [28]. It is generally accepted that alloying Pt with other transition metals allows improving the reaction rates by tuning the d-band structure of the Pt surfaces to lower the bond strength of the Pt-adsorbates, thus leading to better resistance to poisoning [12,28–32]. Many basic research scientists are currently focusing their attention to obtain catalysts with precursors that provide good electrocatalytic activity using small amounts of noble catalytic metals to lower costs [33–36]. Thus, alloying Pt with other transition metals such as Cu, Fe, Ni and Co, has allowed obtaining catalysts with better performance due to favorable electronic effects together with decreasing the amount of precious metals [14,17,18,28,29,31,33,35,37–46].

Ni-containing Pt-based alloys have been synthesized and tested for the oxygen reduction reaction (ORR) [28,33,35,39,41,47–49], and the CO [18,38], methanol [8,31,37,41,50–53] and ethanol [8,22,29,44–46] oxidation reactions, with generally better results than using Pt/C and the same alloys in the absence of Ni. The oxidation of ethylene glycol and glycerol on one-dimensional Pt_3Ni nanowires and nanorods has been also studied [54], with the conclusion that it presented higher mass and specific activities than Pt/C. This was generally explained by geometric factors related to the Pt-Pt bond length decrease and/or the ligand effect of Ni on Pt. Thus, Zignani et al. [39] obtained carbon-supported Pt_xNi_y catalysts that showed a high electrochemically active surface area (ECSA) and good activity towards ORR in acidic medium as compared to commercial Pt/C. Similar results together with good stability were reported by Beermann et al. [28] and Choi et al. [33] with Rh-doped and halide-doped PtNi alloys, respectively. In addition, the methanol tolerance of PtNi alloy cathodes in DMFCs was better than that of Pt/C [41]. On the other hand, alloying the PtRu catalysts with Ni improved their activity for CO, methanol and ethanol oxidation reactions [18,31,38]. Thus, Park et al. [31] reported onset potentials por the MOR decreasing in the sequence: Pt/C > Pt_1Ni_1/C > Pt_1Ru_1/C > $Pt_5Ru_4Ni_1$/C. Wang et al. [45] and Ribadeneira et al. [46]

found that $Pt_{60}Ru_{30}Ni_{10}$/C and $Pt_{75}Ru_{15}Ni_{10}$/C, respectively, performed better than Pt_1Ru_1/C for the EOR. The same was reported for the PtRh alloys used for the ethanol oxidation [29,44]. Erini et al. [44] found that the EOR activity of $Pt_{26}Rh_5Ni_{69}$ outperformed the benchmark $Pt_{32}Rh_{12}Sn_{56}$/C in acidic and alkaline media, with higher specific currents per mass of precious metals than the latter. Shen et al. [29] reported for PtRh catalysts supported on graphene nanosheets that the onset potential for the EOR in $Pt_{75}Rh_{15}Ni_{10}$ was better than that of $Pt_{75}Rh_{25}$. In these papers, catalytic structures mainly consisting of alloys in the form of *fcc* Pt solid solutions have been described.

There are other research papers dealing with core-shell structures [18,37]. Serrà et al. [37] used CoNi nanorods covered by a Pt shell formed by galvanic displacement for the MOR, which presented much better performance than Pt nanorods and Pt/C. Wang et al. [18] reported core-shell structures for the CO oxidation. In this case, a carbon-supported PtNi alloy core covered with a PtRu shell was prepared by impregnation and high temperature reduction, followed by galvanic displacement and annealing treatment. This structure showed higher activity than that of PtRu/C due to the synergistic effect between core and shell. In the latter core-shell structures, Ni did not appear to be in contact with the electrolyte. However, it is under discussion whether the surface Ni is being dissolved during the stability tests [28,33] and/or it is oxidized to highly conductive $Ni(OH)_2$, which may help the desorption of CO by the bifunctional mechanism [38,51]. Recently, Glüsen et al. [49], using dealloyed PtNi/C catalysts with a PtNi core and a Pt-rich shell, found that Ni was necessary in the core and detrimental in the shell for both, the activity and stability of the DMFC cathode. Recent publications show the renewed interest in studying PtNi alloys for methanol oxidation [49,51–54].

In this study, Pt(Ni)/C and PtRu(Ni)/C electrocatalysts on Vulcan XC72R carbon were synthesized using different proportions of metals by chemical reduction of a Ni precursor with $NaBH_4$ and subsequent deposition of Pt from a Pt(IV) precursor. It is then expected that the final structure was a Ni-rich core covered by a Pt-rich shell, similarly to the Pt(Cu)/C and PtRu(Cu)/C catalysts prepared earlier by the authors, which led to good onset potentials for the CO oxidation and the MOR [14,17,42,43]. The catalysts obtained were evaluated in a three-electrode cell for the oxidation reactions of CO and methanol in sulfuric acid. The characterization of the catalysts obtained was performed using the electrochemical methods of cyclic voltammetry (CV), CO stripping and linear sweep voltammetry (LSV). In addition, they were analyzed by X-ray diffraction (XRD), transmission electron microscopy (TEM), energy-dispersive X-ray spectroscopy (EDS) and high-resolution TEM (HRTEM).

2. Results and Discussion

2.1. Electrochemical Characterization by CV

Preliminary experiments showed that the cyclic voltammograms for the catalysts prepared from Pt(IV):Ni(II) ratios of the precursors of 1:1 and 2:1 in weight presented small current densities referred to the electrode section and thus, small hydrogen adsorption/desorption charges. These values were greater for Pt(IV):Ni(II) ratios of 3:1 and 8:1. This can be explained by the different number of Pt active sites in each specimen, which were smaller in the case of 1:1 and 2:1 due to an insufficient amount of Pt to effectively cover the Ni cores. Representative cyclic voltammograms in deaerated 0.5 M H_2SO_4 in the range from −0.2 to 0.8 V of the Pt(Ni)/C catalysts with precursor ratios of 3:1 and 8:1, which will be designed in the following lines as Pt(Ni)/C 3:1 and 8:1, respectively, are depicted in Figure 1, curves *a* and *b*, respectively. As can be seen, the cyclic voltammograms of the Pt(Ni)/C catalysts presented the typical features of Pt/C (curve *c*) [7,17,55,56]: (i) the hydrogen adsorption/desorption region on the (110) and (100) Pt faces (from −0.2 to about 0.2 V), (ii) the Pt oxidation (from ca. 0.45 V) and (iii) the corresponding Pt oxide reduction peak (at about 0.6 V). Note that they have been normalized to the respective hydrogen desorption charge, which is proportional to the number of active sites of the corresponding catalyst, thus allowing a better comparison of their profiles with that of Pt/C. The Pt(Ni)/C catalysts presented cyclic voltammograms with similar profile in the hydrogen adsorption/desorption potential

region as that of commercial Pt/C, which is the expected result when a core shell Pt(Ni) catalyst structure is approached. However, the corresponding peaks in Pt(Ni)/C appear to be somewhat deformed with respect to those of Pt/C, probably due to the conditioning effect of the Ni core on the surface Pt. Some more differences appear in the potential region of Pt oxidation. Pt is oxidized from about 0.45 V in Pt(Ni)/C, whereas it is from about 0.6 V for Pt/C. In addition, the cathodic peak corresponding to Pt oxide reduction appears at about 0.6 V for Pt(Ni)/C, but it is somewhat shifted in the negative direction for Pt/C.

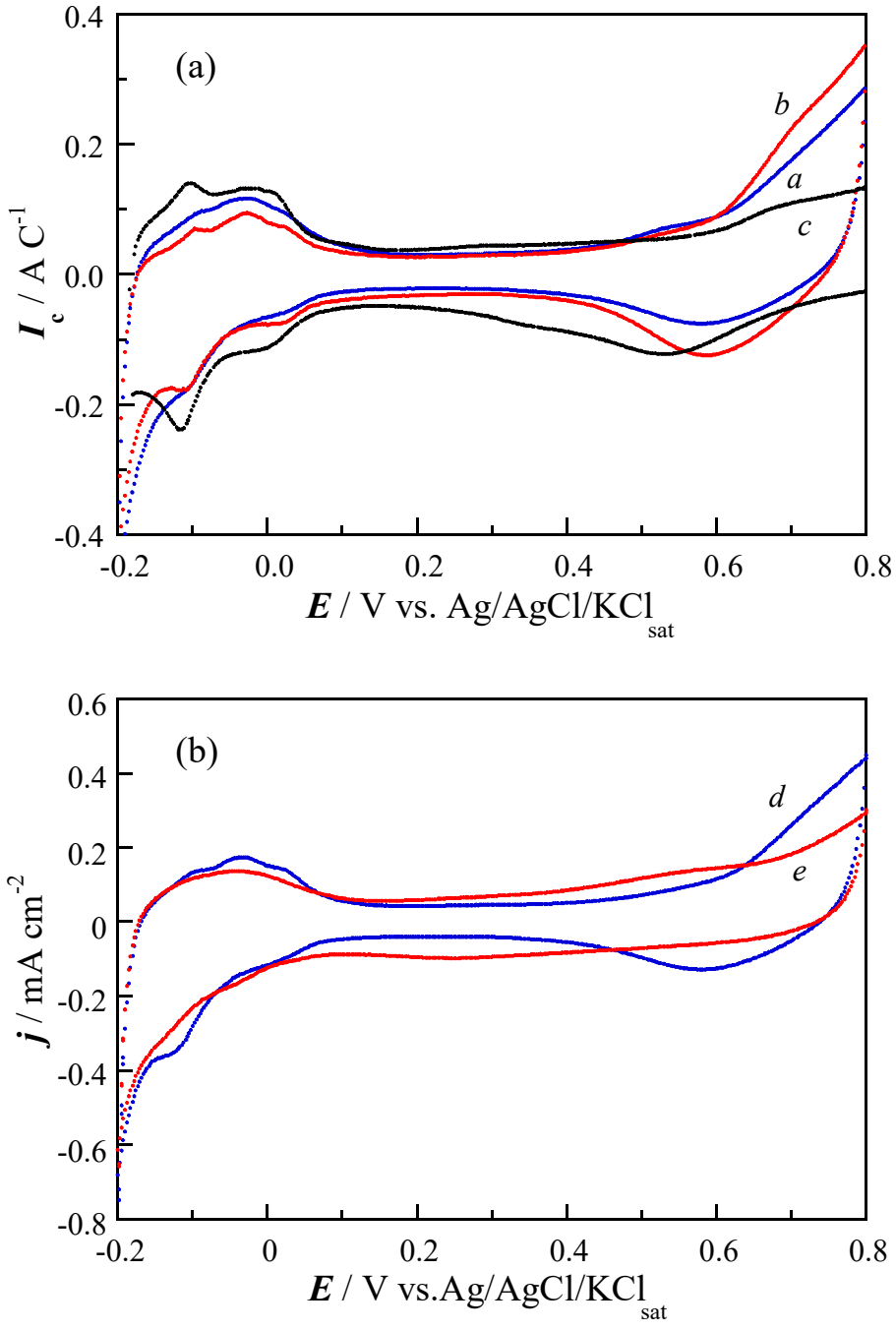

Figure 1. *Cont.*

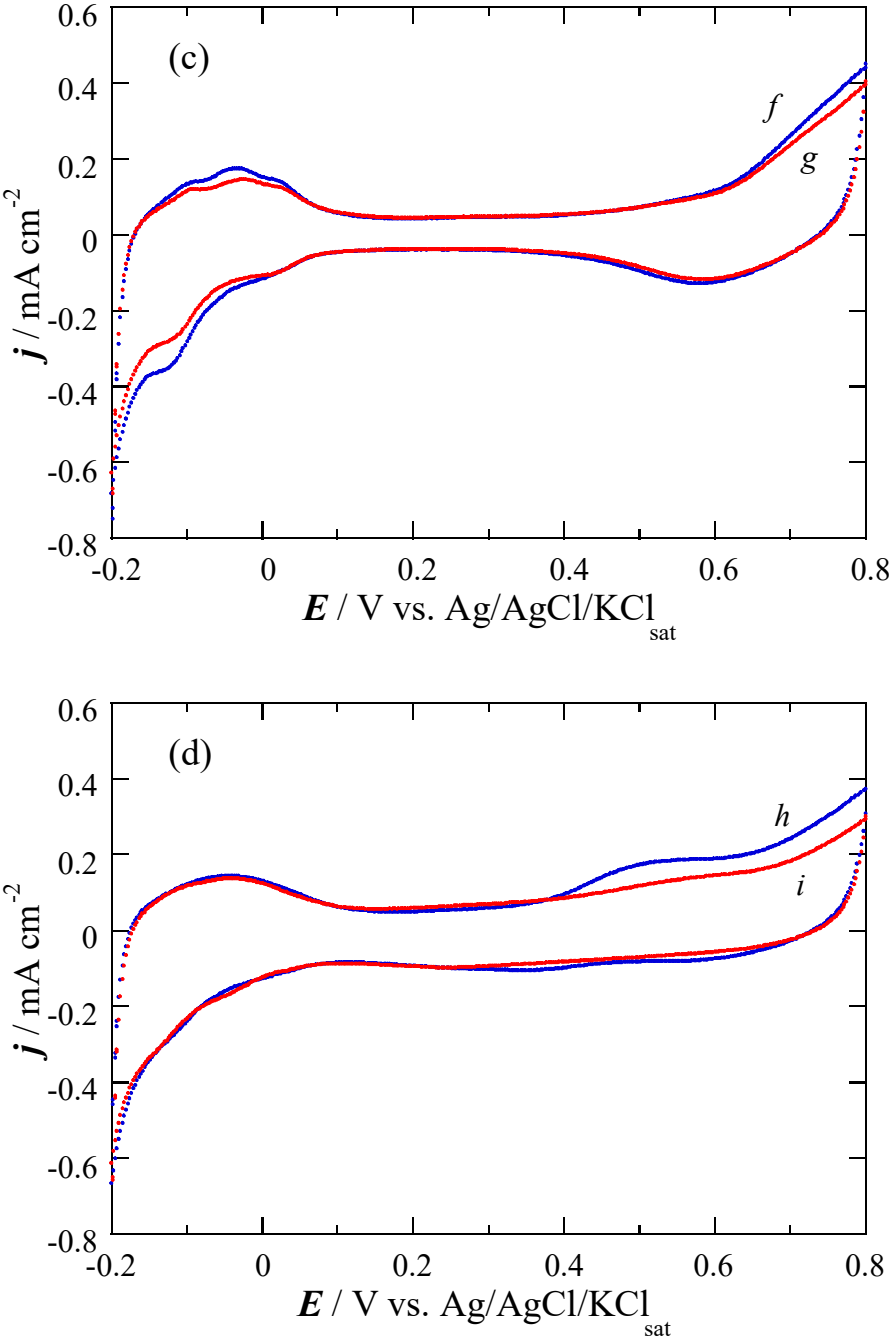

Figure 1. Cyclic voltammograms in deaerated 0.5 M H_2SO_4 of (**a**) Pt(Ni)/C 3:1 (curve *a*) and 8:1 (*b*), compared to Pt/C (*c*); (**b**) Pt(Ni)/C 3:1 (curve *d*) compared to that of PtRu(Ni)/C 3:1 (*e*); (**c**) Pt(Ni)/C 3:1, 1st cyclic voltammogram (curve *f*) compared to the 100th one (*g*); and (**d**) PtRu(Ni)/C 3:1, 1st cyclic voltammogram (curve *h*) compared to the 100th one (*i*) In (**a**) the curves are normalized to the hydrogen desorption charge. In (**b**–**d**), the current densities are relative to the electrode section. Sweep rate 20 mV s^{-1}.

The same trend was reported in our previous paper in which a Pt(Cu)/C was also synthesized by sequenced deposition of Cu and Pt [17]. The onset potential for Pt oxidation in Pt(Cu)/C under the same conditions as in this work was also 0.45 V and the Pt oxide reduction peak was also found at about 0.6 V. This can be interpreted in the same form as in the case of Pt(Cu)/C [17], assuming that the Pt(Ni) nanoparticles present Pt surface structures that are more defective than those found in the lattice of the pure Pt nanoparticle and consequently, the Pt surface atoms are more active in Pt(Ni).

The effect of the spontaneous deposition of Ru species onto Pt(Ni)/C is exemplified in Figure 1b. This figure, in which the current densities referred to the electrode section have been represented, compares the cyclic voltammograms of Pt(Ni)/C 3:1, without (curve *d*) and with deposited Ru species (*e*). As indicated in the experimental part, both specimens were prepared to have the same Pt load. Both curves show similar profiles and are the same as that of Pt (Figure 1a), but the current densities for PtRu(Ni)/C in the potential range of hydrogen adsorption/desorption region are smaller than in Pt(Ni)/C due to the blockage of Pt active sites by the deposited Ru species [11]. As the latter are inactive for hydrogen adsorption, the ECSA of PtRu(Ni)/C is smaller than that of Pt(Ni)/C. In addition, the current densities in the intermediate potential region of 0.1–0.5 V are higher for PtRu(Ni)/C because the capacitive currents increase due to the formation of hydroxylated Ru species. In the potential region of 0.6–0.8 V the current densities are again smaller due the blockage of Pt active sites, which results in a less amount of Pt exposed to oxidation. When comparing the hydrogen adsorption/desorption charges, that corresponding to PtRu(Ni)/C is 80% of Pt(Ni)/C, thus indicating that the coverage of the Pt active sites in the former is 0.20. A very similar value has been obtained for PtRu(Ni)/C 8:1, with a coverage of 0.21 by the Ru species. According to our previous work [11], these values are in the optimum range 0.2–0.3 for CO and methanol electrooxidation. It is worth to note that such small coverages lead to only 0.3 at% of Ru to the PtRu(Cu)/C nanoparticles [17], but it was sufficient to produce major effects in the methanol and the CO electrooxidation.

The cyclic voltammograms were reproducible and repetitive after the first cycle. However, in order to have a first approach to the stability of the catalysts, many consecutive cyclic voltammograms were performed. The first and the 100th cyclic voltammograms for Pt(Ni)/C and PtRu(Ni)/C 3:1 at 20 mV s^{-1} are depicted in Figure 1c,d, respectively. It is shown in these figures that the 1st and 100th cyclic voltammogram of Pt(Ni)/C (curves *f* and *g*), and of PtRu(Ni)/C (curves *h* and *i*), have the same profiles, although a slight decrease in the current densities of the latter is apparent. The hydrogen desorption charges after the consecutive cycling of Pt(Ni)/C and PtRu(Ni)/C 3:1 decreased by 8.8 and 3.0% respectively, with comparable values of 10.5 and 5.0% for 8:1. This can be due to the surface Pt restructuration because the anodic limit of the cyclic voltammograms is well in the potential range of Pt oxidation and therefore, the catalysts can be considered rather stable [43], thus suggesting that Ni is reasonably covered by a Pt shell.

2.2. Structural Analysis

The XRD diffractograms of the Pt(Ni)/C catalysts studied are plotted in Figure 2a, where they are compared to that of Pt/C. The diffraction angles of pure Pt have been also depicted in this figure. Four peaks for the Pt(Ni)/C specimens centered at 2θ angles of 39.8, 46.2, 67.6 and 81.4° appear, which can be related to the (111), (200), (220) and (311) planes of *fcc* Pt [57]. The diffraction angles of the Pt(Ni)/C specimens are only slightly shifted to smaller values with respect to pure Pt, with reported 2θ values of 40.04, 46.54, 67.86 and 81.51° [58], indicating that the Pt-based structures in Pt(Ni)/C are mainly composed of pure Pt. In addition, no diffraction peaks can be ascertained in relation to possible Ni-based phases, which should appear in the positions represented in Figure 2b. If present, they should be as very small crystallites or in amorphous form. Figure 2b is a magnification of the region corresponding to the (111) diffraction peak of Pt, which include the 2θ signals of the (010) and (002) planes of the Ni hexagonal structure at 39.10 and 41.53°, respectively, and also that of the (111) plane of cubic Ni, with a 2θ value of 44.37° [58].

In order to estimate the alloying degree between the involved metal atoms, the Vegard's law is normally applied. However, this law cannot be applied in our case because the Pt-based peaks of the Pt(Ni)/C catalysts are shifted to angles slightly smaller than that of pure Pt. If a *fcc* PtNi alloy was formed, 2θ should be displaced to higher angles, which would correspond to a Pt lattice contraction [18,28,35,39]. In Figure 2, the Pt diffraction peaks are shifted towards the diffraction angle of hexagonal Ni instead to the higher angles where the cubic Ni signal is located. Studies about PtNi catalysts in the literature, prepared by simultaneous reduction of the platinum and nickel

precursors [18,28,33,39,49,51,52,59], described *fcc* alloy structures with 2θ angles between those of pure cubic Pt and pure cubic Ni, then higher than those of Pt, according to a Pt lattice contraction, just the opposite found in this paper. This can be explained assuming that hexagonal Ni is spontaneously formed when depositing Ni alone in the present synthesis conditions, whereas cubic PtNi results from Pt and Ni codeposition.

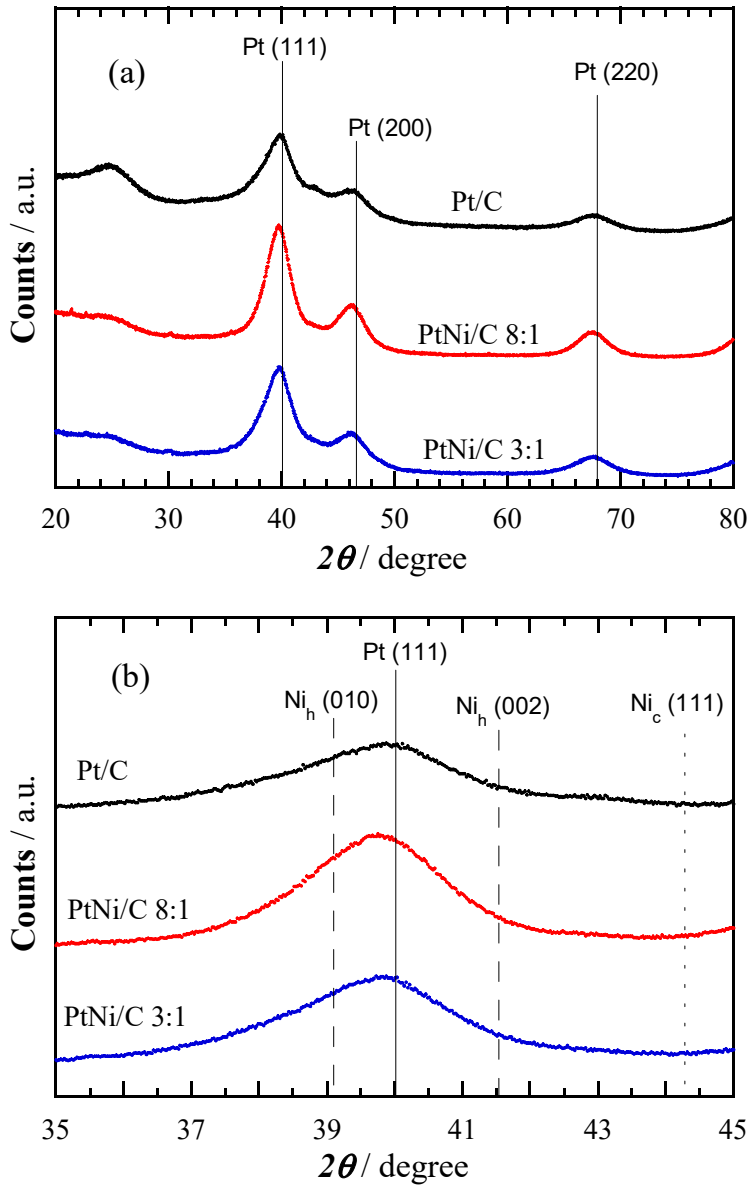

Figure 2. (**a**) XRD diffractograms of the catalysts studied, where that of Pt/C has been included for comparison. (**b**) Magnification of the XRD profiles shown in (**a**) in the Pt (111) 2θ region, including the diffraction angles of hexagonal and cubic Ni.

A Pt lattice contraction was found for Pt(Cu)/C catalysts prepared in the same form as in our present paper, thus indicating some alloying degree between Pt and Cu, forming a *fcc* PtCu alloy structure [43,60]. As this is not the case from the results shown in Figure 2, we may conclude that a PtNi alloy is not being formed in the present conditions. The probable structure of the synthesized Pt(Ni) nanoparticles is composed of very small Ni core with hexagonal structure covered by a Pt shell with cubic structure. We feel that the position of the Pt peaks in Figure 2 could be explained in two forms: (*i*) the Pt lattice is slightly expanded because it has grown on the hexagonal Ni core and (*ii*)

this peak is the summation of the contribution of small hexagonal Ni crystallites together with the dominant Pt cubic phase.

From the Pt diffraction angles, the crystallite sizes have been estimated using the Scherrer Equation (2) and collected in Table 1:

$$d = \frac{K\lambda}{B\cos\theta} \quad (2)$$

where $K = 0.9$, λ (nm) is the wavelength of the X-ray radiation and B (radians) is the width of the measured diffraction peak at an intensity equal to half the maximum one.

Table 1. Mean crystallite size (from XRD), mean particle size (from TEM), composition (from EDS) and ECSA of the Pt(Ni)/C catalysts, compared to commercial Pt/C.

Catalyst	Crystallite Size/nm	Particle Size/nm	Pt Content/wt%	Ni Content/wt%	Pt:Ni/at%	ECSA [a] $/m^2$ g^{-1}
Pt(Ni)/C 3:1	2.4 ± 0.4	2.7 ± 0.5	15.1 ± 2.3	0.62 ± 0.11	88:12	47.8
Pt(Ni)/C 8:1	2.7 ± 0.5	3.5 ± 0.7	19.3 ± 2.8	0.11 ± 0.03	98:2	31.5
Pt/C	2.2 ± 0.5	2.6 ± 0.5	19.0 ± 1.1	0.0	100:0	74.5

[a] Relative error about 5%.

Representative TEM images of the specimens at different magnifications are given in Figure 3. Figure 3a and c show the homogeneous dispersion of the Pt(Ni) nanoparticles on carbon, whereas Figure 3b and d depict the corresponding HRTEM images. The size distribution has been included in the insets of Figure 3a,c, with the mean values also listed in Table 1. They are somewhat higher than those estimated from XRD, but this can be due to the difficulties is ascertaining from the TEM observations the real form of the nanoparticles and their possible aggregation.

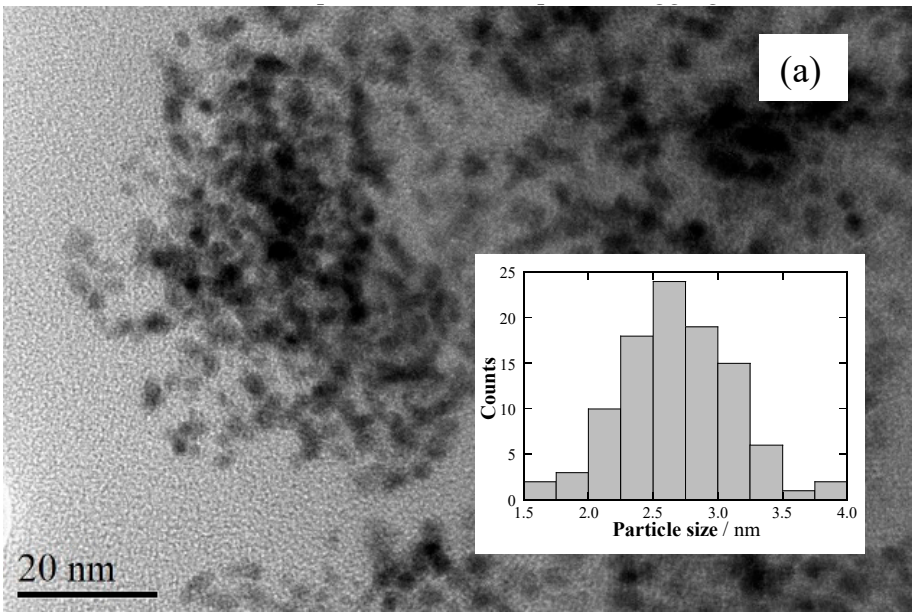

Figure 3. *Cont.*

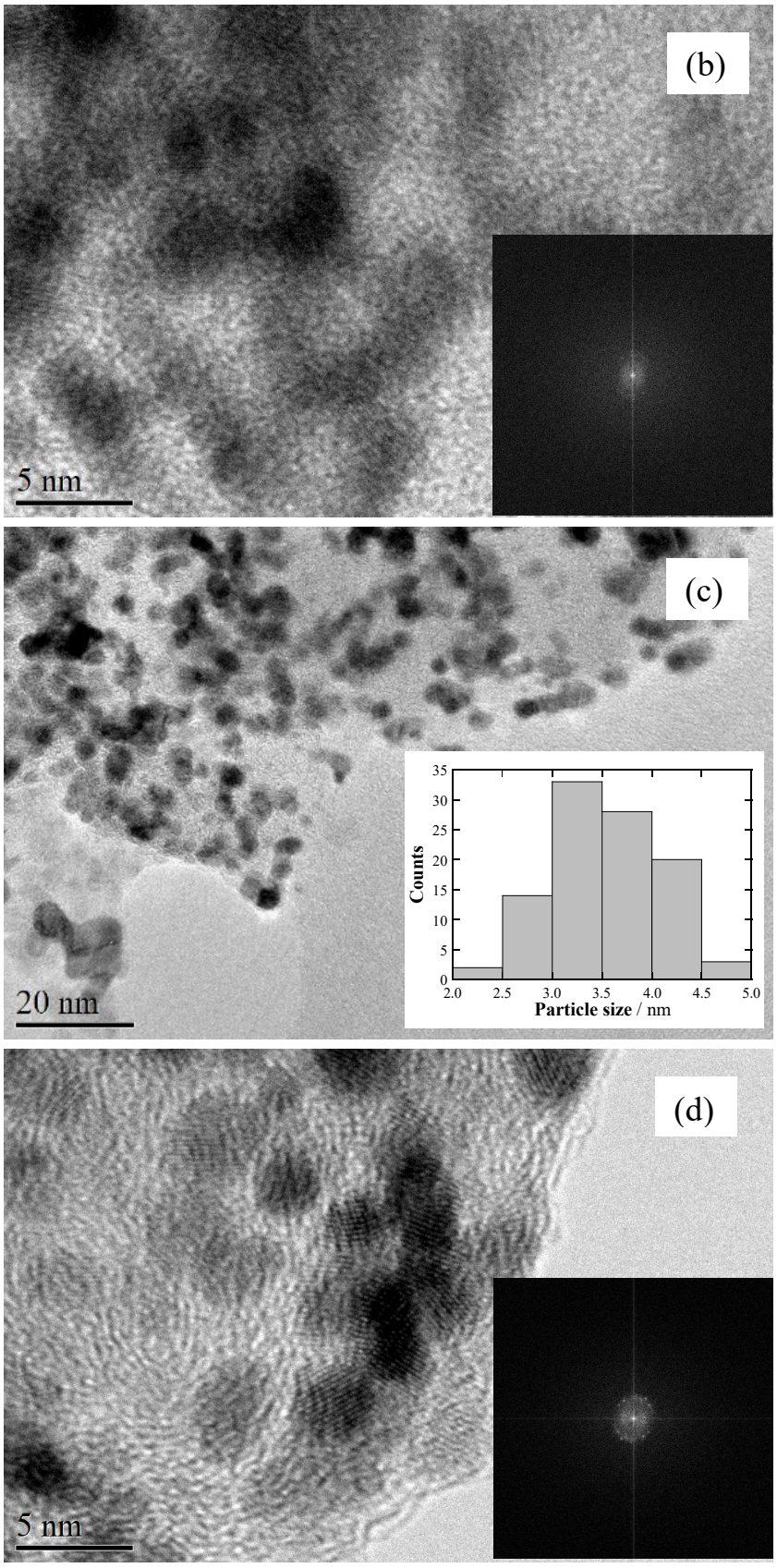

Figure 3. TEM pictures and size distribution of the nanoparticles of (**a**) Pt(Ni)/C 3:1 and (**c**) Pt(Ni)/C 8:1. The high resolution images of Pt(Ni)/C 3:1 and Pt(Ni)/C 8:1 are given in (**b**,**d**), respectively, together with the corresponding FFT pictures presented in the insets.

The Fast Fourier Transform (FFT) analyses given in the inset of Figure 3b reveal *d*-spacings of 2.32, 2.29 and 2.26 Å for the 3:1 precursor ratio, whereas that of Figure 3d, *d*-spacings of 2.35, 2.30, 2.25 and 1.96 Å for 8:1. These values are comparable to the *d*-spacings of 2.25 and 1.95 Å for cubic Pt and to 2.30, 2.17 and 2.03 Å for hexagonal Ni [58]. Cubic Ni should contribute with *d*-spacings of 2.04 and 1.77 Å and seems to be not relevant in this case, in agreement with the XRD results of Figure 2. On the other hand, the EDS analyses performed in STEM mode on different regions of the catalysts were similar, indicating a homogenous dispersion, and led to the mean values also listed in Table 1. It can be observed that the Pt contents in the Pt(Ni)/C catalysts are relatively high, with about 15 and 19 wt% for the 3:1 and 8:1 precursor ratios, respectively, and comparable to commercial Pt/C. The respective amounts of Ni were rather small, of about 0.6 and 0.1 wt%, which corresponded to relative Pt:Ni at% ratios of 88:12 and 98:2. Despite Pt clearly dominated, the TEM results also suggested the presence of small hexagonal Ni structures together with cubic Pt, in agreement with the XRD results. Due to the higher amount of Pt, the possibility that the Pt peaks in Figure 2 to be the summation of the contribution of small hexagonal Ni crystallites together with the dominant Pt cubic phase is more feasible.

2.3. CO Electrooxidation

The cyclic voltammograms corresponding to CO stripping experiments of the Pt(Ni)/C catalysts are depicted in Figure 4a. It is shown that the current-voltage profiles for both, Pt(Ni)/C 3:1 (curve *a*) and 8:1 (curve *b*) present peak potentials that are shifted to potentials more negative than that corresponding to Pt/C (curve *c*). This is related to the different onset potentials, which were about 0.38 and 0.44 V for Pt(Ni)/C 3:1 and 8:1, respectively, whereas that for Pt/C was about 0.48 V. Moreover, the CO stripping peaks in the Pt(Ni)/C catalysts can be deconvoluted into two contributions, with a shoulder at about 0.50 V and a peak at about 0.56 V, whereas only one peak at about 0.60 V appeared in the case of Pt/C. These two contributions for the Pt(Ni)/C catalysts suggest that CO oxidation takes place on two different surface Pt domains having different activity. Both show onset potentials placed at more negative values than that of Pt/C, meaning that more active structures for CO oxidation have been formed in Pt(Ni)/C. This can be explained by the formation of two different domains, one being Ni-rich, in which Ni is covered by a thin layer of Pt, and another one which is Pt-rich, consisting of a thicker layer of Pt on Ni. The peak potential of 0.6 V can be assigned to CO oxidation on Pt (100) and (111) terrace sites [55], which is consistent with the CV profile of Pt/C shown in Figure 1, curve *c*. According to this figure, the Pt(Ni) nanoparticles appeared to have Pt sites of the same type as those of pure Pt and for this reason, we may conclude that the negative shift of the onset potentials to more negative values for the Pt(Ni)/C catalysts was at least due to the electronic effect of Ni. In fact, Park et al. [31] have reported electronic effects of Ni on Pt in PtNi alloys with 1:1 and 3:1 atomic ratios, evidenced by the Pt 4*f* band shift of Pt to smaller binding energies due to the electronic donor effect of Ni. In addition, computational calculations of Jiang et al. [50] showed partial charge transfer from Ni to Pt in Pt_mNi_n alloy clusters, which was supposed to be responsible for the decreased CO poisoning. On the other hand, Corona et al. [32] reported the binding energy tuning of oxygen species with Pt for Pt(Ni) core-shell structures, thus increasing the activity for the oxygen reduction reaction. As a result, Ni in Pt(Ni) produces a positive effect in increasing the CO tolerance of Pt. It is also of interest to note that the onset potential for CO stripping in Pt(Cu)/C catalysts previously studied by us, obtained also by sequenced deposition, was about 0.4 V [17,42], a value close to that of Pt(Ni)/C, curve *a* in Figure 4a. This highlights that Ni and Cu behave in a similar manner in both catalysts. There is however, a significant difference in the onset potentials of Pt(Ni)/C 3:1 and 8:1, which can be the result of the different Pt:Ni atomic ratio in the Pt(Ni) catalysts, as found from the EDS analyses. Pt(Ni)/C 3:1 has higher amount of Ni than 8:1 and therefore, a greater quantity of Ni-rich domains is expected, thus explaining why the peak appearing at the most negative potential is more pronounced than in the latter.

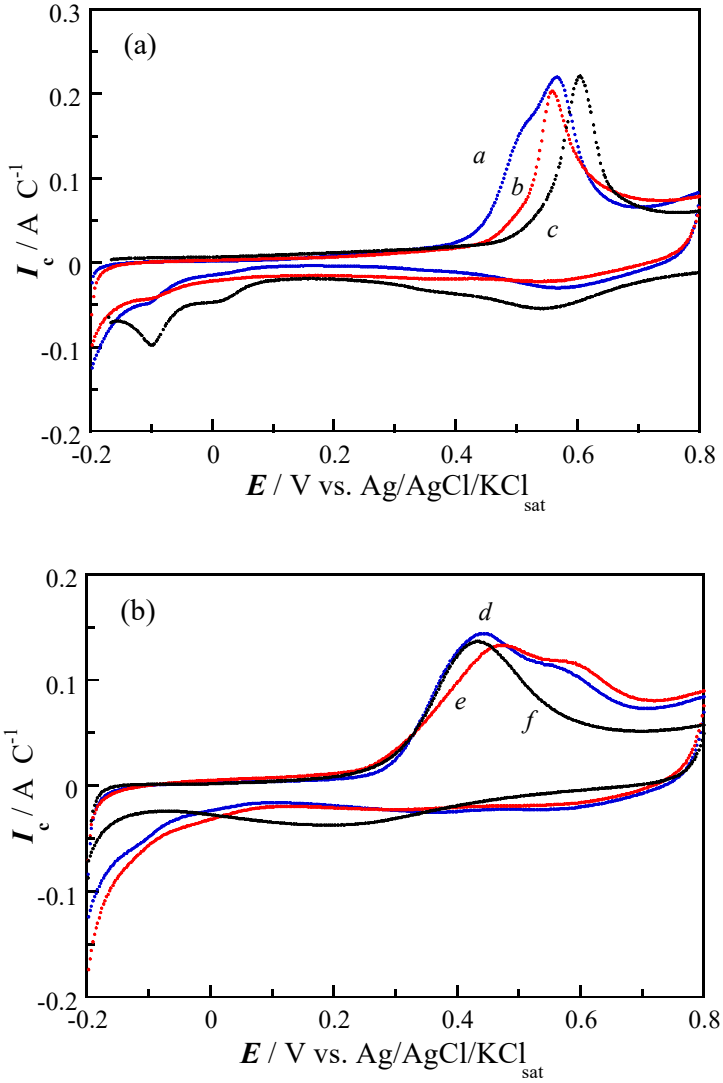

Figure 4. CO stripping experiments on the different catalysts in deaerated 0.5 M H_2SO_4. (**a**) Pt(Ni)/C 3:1 (curve *a*) and 8:1 (*b*), compared to Pt/C (*c*). (**b**) PtRu(Ni)/C 3:1 (curve *d*) and 8:1 (*e*), compared to commercial PtRu/C (*f*). Curves normalized to the CO stripping charge. Sweep rate 20 mV s^{-1}.

From all these results, the positive effect of Ni in the CO tolerance of Pt can be explained by the electronic effect of charge transfer to Pt (ligand effect), which weakens the CO adsorption strength. It is worth mentioning that oxidized Ni species have also been suggested to facilitate the CO oxidation reaction via hydrogen spillover and the enhanced oxidation of CO by nickel hydroxides [38]. No evidence about the presence of oxidized Ni species has been obtained in this paper because according to the cyclic voltammograms shown in Figure 1, it seems that Ni should be completely covered by Pt. A further discussion about this point is performed from the methanol oxidation results shown below.

It is also interesting to compare the CO stripping experiments obtained with the Pt(Ni)/C catalysts with those for PtRu(Ni)/C and PtRu/C. This is presented in Figure 4b, where the different curves have been also normalized to the CO stripping charge. It is shown that there is only one stripping peak for PtRu/C (curve *c*), with a peak potential of about 0.44 V, whereas there are two peaks at 0.44 and 0.56 V for both, Pt(Ni)/C 3:1 (curve *a*) and 8:1 (curve *b*). In the case of PtRu/C, due to the 1:1 atomic ratio, the active sites for CO oxidation have all similar structural characteristics. This appears to be different for PtRu(Ni)/C, in which two distinct structural regions seem to be present, the first one similar to that of PtRu/C (peak potential of 0.44 V) and the second one, similar to that found for Pt(Ni)/C in Figure 4a

(peak potential of 0.56 V). The most interesting result in Figure 4b is that the onset potentials for CO oxidation for both PtRu(Ni)/C catalysts are close to that of PtRu/C, of about 0.24 V. This represents a shift of about 0.14 and 0.20 V in the negative direction with respect to Pt(Ni)/C 3:1 and 8:1, and of about 0.24 V for PtRu/C with respect to Pt/C, respectively. An additional interesting feature is that this onset potential of about 0.24 V approximately coincides with that of PtRu(Cu)/C catalysts prepared by galvanic exchange of Pt with Cu [17,42].

Liang et al. [38] reported an onset potential for CO stripping in PtRuNi/C with 1:1:1 atomic ratios which was about the same as that obtained for PtRu/C. Wang et al. [18] studied the CO tolerance in PtRu/PtNi/C core shell catalysts synthesized by impregnation and high temperature reduction, followed by galvanic displacement of surface Ni by Ru species and further annealing treatment. The nominal atomic ratio of Pt to Ni was 3, and the onset potential for CO stripping in 0.1 M $HClO_4$ was about the same as that for PtRu/C, also in agreement with our results. However, the use of a PtNi core allowed saving the Pt amount and therefore, the mass specific currents (referred to the unit mass of Pt) were significantly higher. One can then conclude that Ni and Cu behave in a similar manner and that the Ru deposited species play the major role in PtRu(Ni)/C and PtRu(Cu)/C.

The Ru species expected to be deposited on Pt(Ni)/C are the same as those on Pt/C, mainly RuO_2 and hydrous oxides RuO_xH_y, as determined by XPS [61]. In this case, the formation of the hydroxylated species $RuO_xH_y(OH)$ through the following Equation (3) is expected [61,62]:

$$RuO_xH_y + H_2O \rightarrow RuO_xH_y(OH) + H^+ + e^- \quad (3)$$

then being $RuO_xH_y(OH)$ instead of Ru(OH) of Equation (1) the Ru species participating in the bifunctional Equation (4) favoring the CO removal:

$$RuO_xH_y(OH) + Pt\text{-}CO \rightarrow RuO_xH_y + Pt + CO_2 + H^+ + e^- \quad (4)$$

Due to the coverage of surface Pt by the Ru species, CO is easier removed by the bifunctional mechanism and the effect of Ni is not now detected due probably to its relatively small amount. In any case, the presence of Ni allows decreasing the cost of the catalyst because less amount of Pt is used.

2.4. Methanol Electrooxidation

The activity of the catalysts has been compared through the corresponding mass activities j_m (currents per Pt mass) and specific activities j_s (currents per squared cm of Pt), which are particularly useful to compare the catalytic activities when dealing with catalysts having different ECSAs [28,43,47]. They were determined from the catalyst loading on the GCE and the charge of the CO stripping peaks, considering that the oxidation of a CO monolayer on polycrystalline Pt needed 420 μC cm^{-2} [63] leading to the ECSA results also listed in Table 1. Values in the range 50–100 m^2 g^{-1} are quite frequent in the literature and depend on the support employed and the synthesis procedure, which condition the number of nucleation centers for the metal deposition [39,40,43,59]. In our case, the Pt deposition in ethylene glycol proceeds on the previously prepared Ni/C specimens. In these conditions, apart from the Pt(IV) reduction by ethylene glycol, the galvanic exchange of Ni by Pt can also take place according to the following Euqaiton (E^0 = 1.004 V):

$$2\ Ni + PtCl_6^{2-} \rightarrow Pt + 2\ Ni^{2+} + 6Cl^- \quad (5)$$

It is then expected that Pt is mainly deposited on the Ni particles in Ni/C because of such a galvanic exchange and that the interaction between the metals is stronger than that with carbon. This can also explain that the ECSA of Pt(Ni)/C 8:1 is smaller than that of Pt(Ni)/C 3:1 because the smaller amount on Ni in the former can facilitate a greater Pt agglomeration. The higher mean size of the Pt(Ni)/C 8:1 nanoparticles estimated from the TEM analyses with respect to the mean values estimated from XRD is also in agreement with such a higher agglomeration in the latter.

The linear sweep voltammograms obtained for the methanol oxidation on the different catalysts studied are shown in Figure 5, the mass activities j_m in Figure 5a and the specific activities j_s in Figure 5b. It is apparent in Figure 5a,b that Pt(Ni)/C 3:1 (curves *a*) showed the most negative onset potentials of about 0.15 V, in front of those of Pt(Ni)/C 8:1 (curves *b*) and Pt/C (curves *c*), with respective onset potentials of about 0.25 and 0.30 V. The improved onset potentials for Pt(Ni)/C with respect to Pt/C correlated with their higher mass and specific activities depicted in Figure 5a,b. This cannot be assigned to the ability of Ni itself for the MOR because, at least, the most part of Ni in the Pt(Ni) nanoparticles can be supposed to be occluded by Pt shells. On the other hand, it was evidenced by Macias-Ferrer et al. [50] that carbon-supported Ni did not have catalytic activity for the MOR. These results are also in agreement with those reported in this paper for CO oxidation (Figure 4a), what is not strange because CO appears to be an intermediate in the methanol oxidation [8,64].

It is also shown in the insets of Figure 5a,b the j_m and j_s values of the catalysts at 0.4 V for a better comparison of their activity. Note the highest j_m value of 220 mA mg_{Pt}^{-1} for Pt(Ni)/C 3:1 in front of 75 and 97 mA mg_{Pt}^{-1} for Pt(Ni)/C 8:1 and Pt/C, respectively. The same trend is observed for j_s, with respective values of 0.45, 0.23 and 0.24 mA cm_{Pt}^{-2} for Pt(Ni)/C 3:1, Pt(Ni)/C 8:1 and Pt/C. The difference between both Pt(Ni)/C catalysts could be also explained by their different relative amount of Ni-rich domains, which would be more active for the methanol (and CO) oxidation, and Pt-rich ones, less active for these reactions. The Ni-rich domains should be more abundant in Pt(Ni)/C 3:1 and this correlated with its greater activity. The smaller mass activities found for Pt(Ni)/C 8:1 could be explained by its smaller Ni content, making it more similar to Pt/C. In fact, Guerrero-Ortega et al. [52] reported maximum mass activities at 20 mV s^{-1} in the same electrolyte of about 700 mA mg_{Pt}^{-1} for methanol oxidation in Ni_3Pt alloys, a value greater than that obtained in the present work of about 420 mA mg_{Pt}^{-1}. This difference can be ascribed to the different Ni content and suggests that it can be increased with the amount of Ni. It is also interesting to remark that Wang et al. [51] reported also onset potentials of about 0.1–0.2 V vs. SCE, which is about 0.15–0.25 V vs. $Ag/AgCl/KCl_{sat}$, at a sweep rate of 50 mV s^{-1} in 0.5 M methanol +0.5 M H_2SO_4, for *fcc* PtNi alloys supported on electrochemically reduced porous graphene oxide. The best onset potentials and the maximum current densities were achieved for the Pt:Ni atomic ratio of 1:1, decaying for higher Pt relative contents and also for higher Ni relative contents. The structure and electronic modification of Pt by Ni has always been invoked to explain the favorable effect of Ni in the alloy in front of the MOR, although some effect of the Ni oxidized species has also been considered [31,51,52]. These results points to that there is a scope to optimize the synthesis of the Pt(Ni)/C catalysts of the present paper to obtain better mass activities.

The onset potentials when using PtRu appeared to be better than those obtained with PtNi, as in the case of CO. Considering the potential scale of the $Ag/AgCl/KCl_{sat}$ reference electrode, onset potentials for the MOR in commercial 1:1 PtRu/C in the conditions of the present paper of about 0.10 V were reported by us [65]. Park et al. [31] gave onset potentials in 2.0 M methanol +0.5 M H_2SO_4 at 50 mV s^{-1} of 0.15, 0.07, 0.09, 0.12 and 0.06 V for pure Pt, 1:1 Pt:Ru, 1:1 Pt:Ni, 3:1 Pt:Ni, and 5:4:1 Pt:Ru:Ni alloy nanoparticle catalysts, respectively. It is then demonstrated that the onset potentials for PtNi catalysts may approach those of PtRu ones, but they are still smaller. This is probably related to the mechanism of the methanol oxidation on these different catalysts. To obtain further insight about this point, the *E* vs log j_s plots shown in Figure 6 were performed, from which the anodic Tafel slopes b_a and charge transfer coefficients α_a were obtained and collected in Table 2. Note that the specific current densities j_s corresponded to real current densities because they were referred to the unit area of Pt.

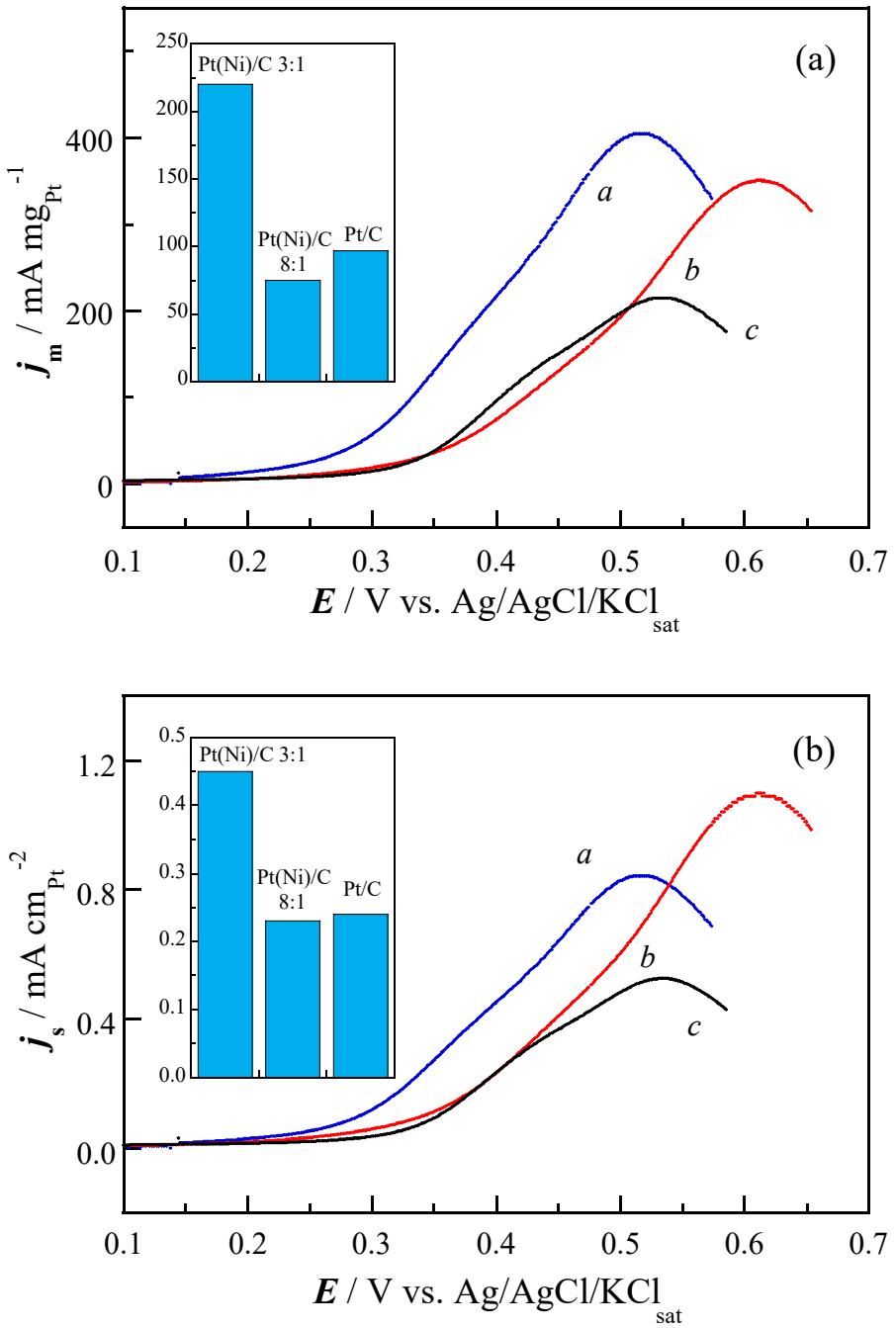

Figure 5. Linear sweep voltammograms obtained for the methanol oxidation in 1.0 M methanol +0.5 M H_2SO_4 on the Pt(Ni)/C 3:1 (curves *a*) and 8:1 (curves *b*), compared to those of Pt/C (curves *c*), corresponding to (**a**) the mass activities j_m and to (**b**) the specific activities j_s. Sweep rate of 20 mV s^{-1}. The j_m and j_s values at 0.4 V are given in the insets.

Good correlation between E and log j_s can be observed, with squared correlation coefficients greater than 0.99. The respective exchange current densities j_{0s}, estimated by extrapolating the Tafel plots to the standard potential of the MOR of −0.153 V vs. Ag/AgCl/KCl_{sat} (0.046 V vs. SHE) [65], are listed in Table 2.

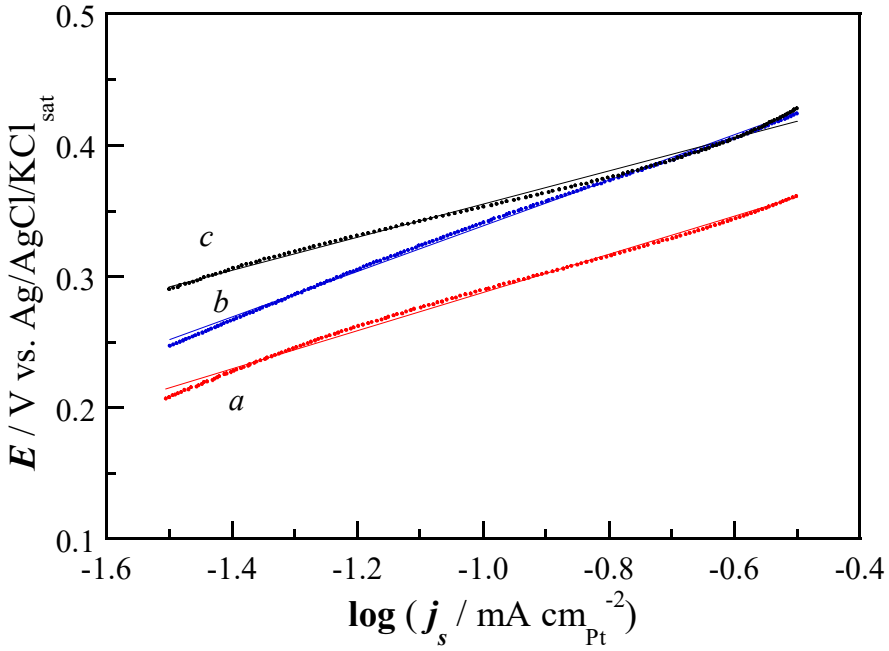

Figure 6. Tafel plots corresponding to the linear sweep voltammograms of Figure 5b. Methanol oxidation in 1.0 M methanol + 0.5 M H_2SO_4 on the Pt(Ni)/C 3:1 (*a*) and 8:1 (*b*) catalysts, compared to that of Pt/C (*c*).

Table 2. Tafel slopes b_a, anodic charge transfer coefficients α_a, and exchange current densities j_{s0} of the MOR, as determined from Figure 6.

Catalyst	b_a/V dec^{-1}	α_a	j_{s0}/mA cm^{-2}
Pt(Ni)/C 3:1	0.150	0.39	1.3×10^{-4}
Pt(Ni)/C 8:1	0.170	0.35	1.2×10^{-4}
Pt/C	0.125	0.48	1.3×10^{-5}

The j_{s0} results clearly evidence that the Pt(Ni)/C catalysts were about ten times more active than Pt/C. The different values of the Tafel slopes and of the anodic charge transfer coefficients also point out to differences in the mechanism for the methanol oxidation on Pt(Ni)/C and Pt/C. The Tafel slope of 0.125 V dec^{-1} and the charge transfer coefficient of 0.48 are close to the values of 0.119 V dec^{-1} and 0.5, respectively, predicted for one electron transfer step as the rate-determining process with the adsorbed intermediates following a Langmuir isotherm [65]. In the case of the methanol oxidation on PtRu/C, in which the hydroxylated species on Ru participated in the bifunctional mechanism, a Tafel slope of 0.199 V dec^{-1} was found, the oxidation of the intermediate CO-type species being proposed as the rate-determining step [65]. Tafel slopes in the range 0.123 to 0.230 V dec^{-1} were also reported in our previous kinetic studies of methanol oxidation on Ru-decorated Pt/C, when the coverage of the Pt sites varied from 0.0 to 0.6, which was attributed to an increase in the amount of the hydroxylated Ru species with coverage [11]. The Tafel slopes and charge transfer coefficients for the MOR on Pt(Ni)/C are intermediate between those found for Pt/C and PtRu/C and suggest that the rate-determining step of the reaction on Pt(Ni)/C is also the oxidation of the intermediate CO-type species. It has been reported in previous studies that $Ni(OH)_2$ plays a role in the CO oxidation and the MOR on PtNi alloys [31,38,51,52], which it is not easily dissolved [28], because it can be oxidized according to Equation (6) [31,38]:

$$Ni(OH)_2 \rightarrow NiOOH + H^+ + e^- \quad (6)$$

and can be recovered by the following redox Equations (7) and (8):

$$NiOOH + x\ Pt\text{-}H \rightarrow Ni(OH)_2 + x\ Pt \quad (7)$$

$$2\ NiOOH + Pt\text{-}CO + H_2O \rightarrow 2\ Ni(OH)_2 + CO_2 + Pt \quad (8)$$

Coming back to the present catalysts it seems improbable that there were significant amounts of $Ni(OH)_2$, considering the cyclic voltammograms of Figure 1 and the overall amount of Ni in the catalysts, as previously discussed. There is in fact the possibility of some $Ni(OH)_2$ formation because the galvanic exchange of Equation (5) leads to Ni^{2+} and in addition, the different structure of Ni and Pt may produce defective Pt/Ni interfaces enabling some Ni oxidation during the anodic scans. However, no significant quantity is expected and the electronic effect of charge transfer (ligand effect) of Ni to Pt is considered the main reason explaining why the activity of Pt(Ni)/C in front of the CO oxidation and the MOR is higher than that of Pt/C. However, these results open the way to further studies analyzing the possible presence and role of oxidized Ni species in Pt(Ni)/C.

3. Materials and Methods

3.1. Synthesis of the Pt(Ni)/C and PtRu(Ni)/C Catalysts

The dispersion of Ni nanoparticles on carbon was prepared by chemical reduction of the Ni(II) precursor with sodium borohydride in basic medium using a procedure adapted from Hosseini et al. [59] and Zignani et al. [39]. The carbon employed was Vulcan XC72R (Cabot Corporation, Boston, MA, USA), which presents a particle size of about 30 nm and a surface area of about 250 $m^2\ g^{-1}$ [17,66], which is frequently used as a support in the literature because its low cost and sufficiently high surface area to obtain a good dispersion of the catalyst nanoparticles. Instead of Pt(IV) and Ni(II) precursors co-reduction, the Ni(II) was reduced first and afterwards, Pt was deposited from a Pt(IV) precursor in order to approach a core-shell structure [43]. First, a carbon dispersion was prepared with 10 mg of carbon, 1.5 mL of isopropyl alcohol (analytical grade, Merck KGaA, Darmstadt, Germany) and 0.5 mL of distilled water, purified by means of a Millipore Direct-Q 3UV-R system ($\varrho > 18.2\ M\Omega$ cm, Merck, Darmstadt, Germany). This mixture was sonicated for 1 h. Then a $NiCl_2$ solution prepared dissolving a given amount of $NiCl_2.6H_2O$ (99.95%, Alfa Aesar, Haverhill, MA, USA) in 1 mL of water was added and further dispersed for 1 h more. The amount of the Ni(II) precursor to prepare 1 mL of such solution was about 10 mg. Afterwards, 0.0165 g of trisodium citrate (analytical grade, Merck KGaA, Darmstadt, Germany) dissolved in 1 mL of water was added to the mixture as a stabilizing agent. Finally, a solution prepared with 0.0337 g of $NaBH_4$ (analytical grade, Merck KGaA, Darmstadt, Germany) and 0.0050 g of NaOH (analytical grade, Alfa Aesar, Haverhill, MA, USA) in 5 mL of water was added dropwise with vigorous stirring at 75 °C. The Ni hydrosol was aged for 24 h at 70 °C in open oven to decompose the residual $NaBH_4$ and obtain dry powder.

The resulting Ni/C powder was dispersed in 3.5 mL ethylene glycol (analytical grade, Alfa Aesar, Haverhill, MA, USA) for 2 h and then, the corresponding amount of 10 wt.% H_2PtCl_6 solution (3 wt.% Pt) (analytical grade, Merck KGaA, Darmstadt, Germany) was added. The amount of the Pt(IV) precursor employed depended on the catalyst to be synthesized, varying between 1:1 and 8:1 the relative content in weight of Pt to Ni in the Pt(IV):Ni(II) precursor ratios. The pH of the mixture was adjusted to a value in the range 7.0–8.0 and it was then stirred for 4 h at 90 °C. The Pt(Ni)/C electrocatalyst was collected after washing with water and then oven dried at 80 °C.

On the basis of the synthesized Pt(Ni)/C catalysts, the PtRu(Ni)/C ones were prepared by spontaneous deposition, as indicated elsewhere [17]. To obtain these catalysts, 1.0 mg mL^{-1} dispersion of Pt(Ni)/C in a 1:1 mixture by volume of isopropanol/water was prepared. Then, 40 μL of this dispersion were placed on the tip of a clean glassy carbon electrode (GCE) and dried under a lamp. Afterwards, the modified electrode was introduced into an aged 8.0 mM solution of $RuCl_3$ in 0.10 M $HClO_4$ (analytical grade Alfa Aesar, Haverhill, MA, USA and Merck, Darmstadt, Germany, respectively)

for 30 min without stirring to carry out the spontaneous deposition of Ru species [17]. This immersion time was selected because in these conditions, intermediate coverage values of the Pt sites by Ru species, suitable for CO and methanol oxidation, were obtained [10,17,67]. Accordingly, PtRu(Ni)/C is mainly Pt(Ni)/C with Ru species on the surface. After careful rinsing with water, the PtRu(Ni)/C catalyst was ready for testing.

3.2. Structural Analyses

The Pt(Ni)/C catalysts were characterized by means of XRD with a PANalytical X'Pert PRO MPD θ/θ powder diffractometer (Cu anode, 45 kV, 40 mA, Malvern Panalytical Ltd., Malvern, UK), using a Cu K_α-filtered radiation (λ = 1.5418 Å), 2θ step size of 0.026° and a measuring time of 200 s per step. The powder of the samples to be analyzed were sandwiched between 3.6-μm thick polyester films.

The samples were examined by TEM using a Hitachi H-800 MT electron microscope (Chiyoda, Tokyo, Japan), which was provided with an EDS detector for the elemental analyses, and by HRTEM with a 200 kV JEOL JEM 2100 F (Akishima, Tokyo, Japan). The elemental analyses by EDS was performed on five different representative zones, taking the average with the experimental error. The size distribution was determined from TEM by counting more than one hundred nanoparticles. The high-resolution pictures, recorded in a Gatan Multiscan 794 charge-coupled device camera, were treated by means of the Gatan Digital Micrograph 3.7.0 software (Pleasanton, CA, USA) to obtain the corresponding FFT images, from which the d-spacing values were determined. To prepare the samples for observation, small amounts of the catalysts were sonicated in 3 mL of n-hexane for 10 min and then, a drop of the dispersion was placed on a holey carbon grid, which was heated with a lamp to evaporate the solvent.

3.3. Electrochemical Testing

The electrochemical characterization was carried out in a conventional three-electrode 100 mL cell (PAR, Ametek, Berwyn, PA, USA) with double wall for thermostatization by means of a PARSTAT (PAR) 3000A potentiostat. The base electrolyte was 0.5 M H_2SO_4 (analytical grade, Merck KGaA, Darmstadt, Germany), deaerated by N_2 purging (99.995%, Praxair, Nippon Gases, Japan). The auxiliary electrode was a rolled Pt wire. The reference electrode was a double junction Ag/AgCl/KCl_{sat} (E = 0.199 V vs. SHE at 25 °C). All the potentials given in this paper have been referred to such a reference electrode. The working electrode was a GCE 5 mm in diameter (0.196 cm^2 in section) GCE (PINE Research Instrumentation, Durham, NC, USA), surface-modified by the catalyst. Prior to the modification, the GCE was polished consecutively with an alumina suspension of 0.3 and 0.05 μm in grain size using a polishing cloth (ALS Co., Ltd., Tokyo, Japan) to achieve specular gloss. Between polishing steps, the electrode was sonicated in water and dried. For the electrochemical testing, amounts of 1.0 mg mL^{-1} of the Pt(Ni)/C catalyst powders were dispersed by sonication in isopropanol/water mixture 1:1 by volume and then, 40 μL of each dispersion were dropped on the GCE, which was further dried by heating with a lamp. In the cell containing deaerated 0.5 M H_2SO_4, the catalyst was submitted to a cleaning protocol by CV consisting in consecutive cycles at 100, 50 and 20 mV s^{-1} in the potential range between −0.2 and 0.8 V up to a stationary profile. The PtRu(Ni)/C catalysts prepared by spontaneous deposition of Ru species were also submitted to the same cleaning protocol.

After the cleaning protocol, the CO electrooxidation activity was analyzed by means of CO stripping voltammograms in 0.5 M H_2SO_4 and the same potential range between -0.2 and 0.8 V at 20 mV s^{-1}. For the CO adsorption, CO gas (Linde 3.0, purity greater than 99.9%, Dublin, Ireland) was bubbled through the solution for 15 min while applying a potential of −0.100 V to the working electrode. The non-adsorbed CO remaining in solution was removed by N_2 bubbling through the solution for 30 min. The activity of the catalysts for the methanol reaction was examined by LSV at 20 mV s^{-1}, starting the scan from −0.2 V. The corresponding tests were performed using deaerated 1.0 M solutions of each alcohol (analytical grade, Panreac Química, Barcelona, Spain) in 0.5 M H_2SO_4. The experiments were repeated three times to test the reproducibility. The corresponding results were

compared to those obtained from commercial 20 wt% Pt/C and 20 wt% 1:1 PtRu/C (Premetek, Cherry Hill, NJ, USA) catalysts.

4. Conclusions

In this paper, the electrochemical performance of Pt(Ni)/C and PtRu(Ni)/C catalysts, synthesized by sequenced deposition of Ni, Pt and Ru to approach core-shell structures, in front of the CO and methanol oxidation reactions has been studied. The best hydrogen desorption charges were obtained for the Pt(Ni)/C alloys with relative amounts in weight of Pt to Ni of 3:1 and 8:1. The EDS analyses indicated 88:12 and 98:2 Pt:Ni atomic ratios in these alloys, respectively, the corresponding ECSAs being of 47.8 and 31.5 $m^2\ g_{Pt}{}^{-1}$. The XRD, HRTEM and FFT analyses pointed out to the formation of small hexagonal Ni crystallites covered by cubic Pt surface structures with no evidence about PtNi alloy formation. Two anodic peaks were found in the CO oxidation on Pt(Ni)/C alloys, thus suggesting the presence of two distinct structural domains in the catalyst surface, probably Pt on hexagonal Ni-rich domains and on cubic Pt-rich ones. The potential shift in the negative direction of about 0.10 V for the onset of CO oxidation in Pt(Ni)/C with respect to Pt/C was explained by the charge transfer of Ni to Pt (ligand effect), which resulted in an easier removal of adsorbed CO, thus increasing the CO tolerance of the catalyst. The onset potential for CO oxidation and tolerance was improved with PtRu(Ni)/C. The effect of surface Ru species spontaneously deposited on Pt appeared to present the major effect by facilitating the CO removal by the bifunctional mechanism. The onset potentials of Pt(Ni)/C 3:1 and 8:1 for the methanol oxidation, which were about 0.15 and 0.05 V lower than that of Pt/C, respectively, depending on the Ni content, also indicated the positive effect of Ni. The mass and specific activities of the Pt(Ni)/C catalysts were also higher than those of Pt/C, with exchange current densities one order of magnitude greater than that of the latter. The experimental Tafel slopes for the MOR on Pt(Ni)/C were higher, and the charge transfer coefficients smaller, than those of Pt/C, thus suggesting different rate-determining steps in the mechanism. The ligand effect of Ni on Pt was also considered the main reason why the activity of Pt(Ni)/C in front of the MOR was higher than that of Pt/C.

Author Contributions: G.C.-M. and P.L.C. conceived and designed the experiments; G.C.-M., J.M.S. and J.G.-C. performed the experiments; G.C.-M., E.B., and P.L.C. analyzed the data; J.A.J. and J.G.-C. contributed reagents/materials/analysis tools; G.C.-M., J.A.J., P.L.C. and E.B. wrote the paper. All authors have read and agreed to the published version of the manuscript.

Funding: The authors thank the financial support from the National Secretariat for Science, Technology, and Innovation of Panama (SENACYT) through the Project FID-16-035 and National Research System (SNI).

Acknowledgments: The authors thank the Scientific and Technological Centers of the University de Barcelona (CCiT-UB) for the TEM and XRD analysis facilities.

Conflicts of Interest: The authors declare no conflict of interest. The funding sponsors had no role in the design of the study; in the collection, analyses, or interpretation of data; in the writing of the manuscript, and in the decision to publish the results.

References

1. Serov, A.; Zenyuk, I.; Arges, C.; Chatenet, M. Hot topics in alkaline exchange membrane fuel cells. *J. Power Sources* **2017**, *375*, 149–157. [CrossRef]
2. Alcaide, F.; Cabot, P.L.; Brillas, E. Fuel Cell for chemicals and energy cogeneration. *J. Power Sources* **2006**, *153*, 47–60. [CrossRef]
3. Cohen, J.; Volpe, D.; Abruña, H. Electrochemical determination of activation energies for methanol oxidation on polycrystalline platinum in acidic and alkaline electrolytes. *Phys. Chem. Chem. Phys.* **2007**, *9*, 49–77. [CrossRef] [PubMed]
4. Demirci, U.B. Direct liquid-feed fuel cells: Thermodynamic and environmental concerns. *J. Power Sources* **2007**, *169*, 239–246. [CrossRef]
5. Ong, B.C.; Kamarudin, S.K.; Basri, S. Direct liquid fuel cells: A review. *Int. J. Hydrogen Energy* **2017**, *42*, 10142–10157. [CrossRef]

6. Apanel, G.; Johnson, E. Direct methanol fuel cells—Ready to go comercial? *Fuel Cells* **2004**, *11*, 12–17. [CrossRef]
7. Vassiliev, Y.B.; Bagotsky, V.S.; Osetrova, N.V.; Khasova, O.A.; Mayorova, N.A. Electroreduction of carbon dioxide: Part I. The mechanism and kinetics of electroreduction of CO_2 in aqueous solutions on metals with high and moderate hydrogen overvoltages. *J. Electroanal. Chem. Interfacial Electrochem.* **1985**, *189*, 271–294. [CrossRef]
8. Puthiyapura, V.K.; Lin, W.F.; Russell, A.E.; Brett, D.J.L.; Hardacre, C. Effect of Mass Transport on the Electrochemical Oxidation of Alcohols Over Electrodeposited Film and Carbon-Supported Pt Electrodes. *Top. Catal.* **2018**, *61*, 240–253. [CrossRef]
9. Spendelow, J.S.; Wieckowski, A. Electrocatalysis of oxygen reduction and small alcohol oxidation in alkaline media. *Phys. Chem. Chem. Phys.* **2007**, *9*, 2654–2675. [CrossRef]
10. Ruth, K.; Vogt, M.; Zuber, R. Development of CO-Tolerant Catalysts. In *Handbook of Fuel Cells-Fundamentals, Technology and Applications*; Vielstich, W., Gasteiger, H.A., Lamm, A., Eds.; John Wiley & Sons: New York, NY, USA, 2003; Volume 3, pp. 489–496.
11. Velázquez-Palenzuela, A.; Brillas, E.; Arias, C.; Centellas, F.; Garrido, J.A.; Rodríguez, R.M.; Cabot, P.L. Carbon monoxide, methanol and ethanol electro-oxidation on Ru decorated carbon-supported Pt nanoparticles prepared by spontaneous deposition. *J. Power Sources* **2013**, *225*, 163–171. [CrossRef]
12. Antolini, E. Effect of the structural characteristics of binary Pt-Ru and ternary Pt-Ru-M fuel cell catalysts on the activity of ethanol electrooxidation in acid medium. *ChemSusChem* **2013**, *6*, 966–973. [CrossRef] [PubMed]
13. Rigsby, M.A.; Zhou, W.P.; Lewera, A.; Duong, H.T.; Bagus, P.S.; Jaegermann, W.; Hunger, R.; Wieckowski, A. Experiment and theory of fuel cell catalysis: Methanol and formic acid decomposition on nanoparticle Pt/Ru. *J. Phys. Chem. C* **2008**, *112*, 15595–15601. [CrossRef]
14. Caballero-Manrique, G.; Brillas, E.; Centellas, F.; Garrido, J.A.; Rodríguez, R.M.; Cabot, P.L. Electrochemical oxidation of the carbon support to synthesize Pt(Cu) and Pt-Ru(Cu) core-shell electrocatalysts for low-temperature fuel cells. *Catalysts* **2015**, *5*, 815–837. [CrossRef]
15. Watanabe, M.; Motoo, S. Electrocatalysis by ad-atoms: Part III. Enhancement of the oxidation of carbon monoxide on platinum by ruthenium ad-atoms. *J. Electroanal. Chem. Interfacial Electrochem.* **1975**, *60*, 275–283. [CrossRef]
16. Brankovic, S.R.; Wang, J.X.; Adzić, R.R. Pt Submonolayers on Ru Nanoparticles: A Novel Low Pt Loading, High CO Tolerance Fuel Cell Electrocatalyst. *Electrochem. Solid-State Lett.* **2001**, *4*, 217–220. [CrossRef]
17. Caballero-Manrique, G.; Velázquez-Palenzuela, A.; Centellas, F.; Garrido, J.A.; Arias, C.; Rodríguez, R.M.; Brillas, E.; Cabot, P.L. Electrochemical synthesis and characterization of carbon-supported Pt and Pt-Ru nanoparticles with Cu cores for CO and methanol oxidation in polymer electrolyte fuel cells. *Int. J. Hydrogen Energy* **2014**, *39*, 12859–12869. [CrossRef]
18. Wang, Q.; Wang, G.; Tao, H.; Li, Z.; Han, L. Highly CO tolerant PtRu/PtNi/C catalyst for polymer electrolyte membrane fuel cell. *RSC Adv.* **2017**, *7*, 8453–8459. [CrossRef]
19. Dinh, H.; Ren, X.; Garzon, F.; Zelenay, P.; Gottesfeld, S. Electrocatalysis in direct methanol fuel cells: In-situ probing of PtRu anode catalyst surfaces. *J. Electroanal. Chem.* **2000**, *491*, 222–233. [CrossRef]
20. Alcaide, F.; Álvarez, G.; Cabot, P.L.; Genova-Koleva, R.V.; Grande, H.J.; Martínez-Huerta, M.; Miguel, O. Supporting PtRh alloy nanoparticle catalysts by electrodeposition on carbon paper for the ethanol electrooxidation in acidic medium. *J. Electroanal. Chem.* **2020**, *861*, 113960. [CrossRef]
21. Iwasita, T.; Pastor, E. A DEMS and FTIR spectroscopic investigation of adsorbed ethanol on polycrystalline platinum. *Electrochim. Acta* **1994**, *39*, 531–537. [CrossRef]
22. Zhou, W.; Zhou, Z.; Song, S.; Li, W.; Sun, G.; Tsiakaras, P.; Xin, Q. Pt based anode catalysts for direct ethanol fuel cells. *Appl. Catal. B* **2003**, *46*, 273–285. [CrossRef]
23. Zignani, S.C.; Baglio, V.; Sebastián, D.; Siracusano, S.; Aricò, A.S. Enhancing ethanol oxidation rate at PtRu electro-catalysts using metal-oxide additives. *Electrochim. Acta* **2016**, *191*, 183–191. [CrossRef]
24. Zhou, W.K.; Zhou, B.; Li, W.Z.; Zhou, Z.H.; Song, S.Q.; Sun, G.Q.; Xin, Q.; Douvartzides, S.; Goula, M.; Tsiakaras, P. Performance comparison of low-temperature direct alcohol fuel cells with different anode catalysts. *J. Power Sources* **2004**, *126*, 16–22. [CrossRef]
25. Zhou, W.J.; Li, W.Z.; Song, S.Q.; Zhou, Z.H.; Jiang, L.H.; Sun, G.Q.; Xin, Q.; Poulianitis, K.; Kontou, S.; Tsiakaras, P. Bi- and tri-metallic Pt-based anode catalysts for direct ethanol fuel cells. *J. Power Sources* **2004**, *131*, 217–223. [CrossRef]

26. Spinacé, E.V.; Dias, R.R.; Brandalise, M.; Linardi, M.; Neto, A.O. Electro-oxidation of ethanol using PtSnRh/C electrocatalysts prepared by an alcohol-reduction process. *Ionics* **2010**, *16*, 91–95. [CrossRef]
27. Macias-Ferrer, D.; Melo, J.A.; Páramo, U.; Silva, R.; Lam-Maldonado, M.; Meraz-Melo, M.A.; Verde-Gómez, J.Y.; Díaz-Zavala, N.P. Pt, Co, Fe and Ni Nanoparticles on Micro/Nano-Structured Carbon for the Methanol Electro-Oxidation in Acid Medium. *AJER* **2018**, *7*, 344–356. [CrossRef]
28. Beermann, V.; Gocyla, M.; Willinger, E.; Rudi, S.; Heggen, M.; Dunin-Borkowski, R.E.; Willinger, M.G.; Strasser, P. Rh-doped Pt-Ni octahedral nanoparticles: Understanding the correlation between elemental distribution, ORR and shape stability. *Nano Lett.* **2016**, *16*, 1719–1725. [CrossRef]
29. Shen, Y.; Zhang, M.Z.; Xiao, K.; Xi, J. Synthesis of Pt, PtRh, and PtRhNi alloys supported by pristine graphene nanosheets for ethanol oxidation. *ChemCatChem* **2014**, *6*, 3254–3261. [CrossRef]
30. Stamenkovic, V.R.; Mun, B.S.; Arenz, M.; Mayrhofer, K.J.J.; Lucas, C.A.; Wang, G.F.; Ross, P.N.; Markovic, N.M. Trends in electrocatalysis on extended and nanoscale Pt-bimetallic alloy surfaces. *Nat. Mater.* **2007**, *6*, 241–247. [CrossRef]
31. Park, K.W.; Choi, J.H.; Kwon, B.K.; Lee, S.A.; Sung, Y.E.; Ha, H.Y.; Hong, S.A.; Kim, H.; Wieckowski, A. Chemical and Electronic Effects of Ni in Pt/Ni and Pt/Ru/Ni Alloy Nanoparticles in Methanol Electrooxidation. *J. Phys. Chem. B* **2002**, *106*, 1869–1877. [CrossRef]
32. Corona, B.; Howard, M.; Zhang, L.; Henkelman, G. Computational screening of core@shell nanoparticles for the hydrogen evolution and oxygen reduction reactions. *J. Chem. Phys.* **2016**, *145*, 244708. [CrossRef] [PubMed]
33. Choi, J.; Lee, Y.; Kim, J.; Lee, H. Enhancing stability of octahedral PtNi nanoparticles for oxygen reduction reaction by halide treatment. *J. Power Sources* **2016**, *307*, 883–890. [CrossRef]
34. Wu, F.; Liu, Y.; Wu, C. Preparation of Pt/C Nanocatalysts by Ethylene Glycol Method in Weakly Acidic Solutions. *J. Mater. Sci. Technol.* **2010**, *26*, 705–710. [CrossRef]
35. Mohanraju, K.; Cindrella, L. One-pot surfactant-free synthesis of high surface area ternary alloys, PtMCo/C (M $\frac{1}{4}$ Cr, Mn, Fe, Ni, Cu) with enhanced electrocatalytic activity and durability for PEM fuel cell application. *Int. J. Hydrogen Energy* **2016**, *41*, 9320–9331. [CrossRef]
36. Stephen, A.; Rees, N.; Mikheenko, I.; Macaskie, L. Platinum and Palladium Bio-Synthesized Nanoparticles as Sustainable Fuel Cell Catalysts. *Front. Energy Res.* **2019**, *7*, 1–13. [CrossRef]
37. Serrà, A.; Gómez, E.; Vallés, E. Novel electrodeposition media to synthesize CoNi-Pt Core@Shell stable mesoporous nanorods with very high active surface for methanol electro-oxidation. *Electrochim. Acta* **2015**, *174*, 630–639. [CrossRef]
38. Liang, Y.; Zhang, H.; Tian, Z.; Zhu, X.; Wang, X.; Yi, B. Synthesis and Structure-Activity Relationship Exploration of Carbon-Supported PtRuNi Nanocomposite as a CO-Tolerant Electrocatalyst for Proton Exchange Membrane Fuel Cells. *J. Phys. Chem. B* **2006**, *110*, 7828–7834. [CrossRef]
39. Zignani, S.; Baglio, V.; Sebastián, D.; Rocha, T.; Gonzalez, E.; Aricò, A. Investigation of PtNi/C as methanol tolerant electrocatalyst for the oxygen reduction reaction. *J. Electroanal. Chem.* **2016**, *763*, 10–17. [CrossRef]
40. Menshchikov, V.; Alekseenko, A.; Guterman, V.; Nechitailov, A.; Glebova, N.; Tomasov, A.; Spiridonova, O.; Belenov, S.; Zelenina, N.; Safronenko, O. Effective Platinum-Copper Catalysts for Methanol Oxidation and Oxygen Reduction in proton-Exchange membrane Fuel Cell. *Nanomaterials* **2020**, *10*, 742. [CrossRef]
41. Antolini, E.; Salgado, J.R.C.; Gonzalez, E.R. Carbon supported Pt75M25 (M = Co, Ni) alloys as anode and cathode electrocatalysts for direct methanol fuel cells. *J. Electroanal. Chem.* **2005**, *580*, 145–154. [CrossRef]
42. Caballero-Manrique, G.; Nadeem, I.; Brillas, E.; Centellas, F.; Garrido, J.A.; Rodríguez, R.M.; Cabot, P.L. Effects of the Electrodeposition Time in the Synthesis of Carbon-Supported Pt(Cu) and Pt-Ru(Cu) Core-Shell Electrocatalysts for Polymer Electrolyte Fuel Cells. *Catalysts* **2016**, *6*, 125. [CrossRef]
43. Garcia-Cardona, J.; Sirés, I.; Alcaide, F.; Brillas, E.; Centellas, F.; Cabot, P.L. Electrochemical performance of carbon-supported Pt(Cu) electrocatalysts for low-temperature fuel cells. *Int. J. Hydrogen Energy* **2020**, in press. [CrossRef]
44. Erini, N.; Rudi, S.; Beermann, V.; Krause, P.; Yang, R.; Huang, Y.; Strasser, P. Exceptional Activity of a Pt–Rh–Ni Ternary Nanostructured Catalyst for the Electrochemical Oxidation of Ethanol. *ChemElectroChem* **2015**, *2*, 903–908. [CrossRef]
45. Wang, Z.B.; Zuo, P.J.; Wang, G.J.; Du, C.Y.; Yin, G.P. Effect of Ni on PtRu/C Catalyst Performance for Ethanol Electrooxidation in Acidic Medium. *J. Phys. Chem. C* **2008**, *112*, 6582–6587. [CrossRef]

46. Ribadeneira, E.; Hoyos, B.A. Evaluation of Pt–Ru–Ni and Pt–Sn–Ni catalysts as anodes in direct ethanol fuel cells. *J. Power Sources* **2008**, *180*, 238–242. [CrossRef]
47. Cui, C.; Gan, L.; Li, H.H.; Yu, S.H.; Heggen, M.; Strasser, P. Octahedral PtNi nanoparticle catalysts: Exceptional oxygen reduction activity by tuning the alloy particle surface composition. *Nano Lett.* **2012**, *12*, 5885–5889. [CrossRef]
48. Stamenkovic, V.R.; Fowler, B.; Mun, B.S.; Wang, G.; Ross, P.N.; Lucas, C.A.; Markovic, N.M. Improved Oxygen Reduction Activity on Pt_3Ni(111) via Increased Surface Site. *Science* **2007**, *315*, 493–497. [CrossRef]
49. Glüsen, A.; Dionigi, F.; Paciok, P.; Heggen, M.; Müller, M.; Gan, L.; Strasser, P.; Dunin-Borkowski, R.E.; Stolten, D. Dealloyed PtNi-Core-Shell Nanocatalysts Enable Significant Lowering of Pt Electrode Content in Direct Methanol fuel Cells. *ACS Catal.* **2019**, *9*, 3764–3772. [CrossRef]
50. Jiang, Q.; Jiang, L.; Hou, H.; Qi, J.; Wang, S.; Sun, G. Promoting Effect of Ni in PtNi Bimetallic Electrocatalysts for the Methanol Oxidation Reaction in Alkaline Media Experimental and Density Functional Theory Studies. *J. Phys. Chem. C* **2010**, *114*, 19714–19722. [CrossRef]
51. Wang, Y.; Yang, J.; Sun, S.; Wang, L.; Guo, T.; Zhang, D.; Xue, Z.; Zhou, X. PtNi nanoparticles supported on electrochemically reduced porous graphene oxide for methanol oxidation reaction. *Chem. Phys. Lett.* **2019**, *730*, 575–581. [CrossRef]
52. Guerrero-Ortega, L.P.A.; Manzo-Robledo, A.; Ramírez-Meneses, E.; Mateos-Santiago, J.; Lartundo-Rojas, L.; Garibay-Febles, V. Methanol electrooxidation reaction at the interface of (bi)-metallic (PtNi) synthesized nanoparticles supported on carbon Vulcan. *Int. J. Hydrogen Energy* **2018**, *43*, 6117–6130. [CrossRef]
53. Wang, C.; Zhang, Y.; Zhang, Y.; Xu, P.; Feng, C.; Chen, T.; Guo, T.; Yang, F.; Wang, Q.; Wang, J.; et al. Highly Ordered Hierarchical Pt and PtNi Nanowire Arrays for Enhanced Electrocatalytic Activity toward Methanol Oxidation. *ACS Appl. Mater. Interfaces* **2018**, *10*, 9444–9459. [CrossRef] [PubMed]
54. Gao, F.; Zhang, Y.; Song, P.; Wang, J.; Yan, B.; Sun, Q.; Li, L.; Zhu, X.; Du, Y. Shape-control of one-dimensional PtNi nanostructures as efficient electrocatalysts for alcohol electrooxidation. *Nanoscale* **2019**, *11*, 4831–4836. [CrossRef]
55. Solla-Gullón, J.; Vidal-Iglesias, F.J.; Herrero, E.; Feliu, J.M.; Aldaz, A. CO monolayer oxidation on semi-spherical and preferentially oriented (100) and (111) platinum nanoparticles. *Electrochem. Commun.* **2006**, *8*, 189–194. [CrossRef]
56. Esparbé, I.; Brillas, E.; Centellas, F.; Garrrido, J.A.; Rodríguez, R.M.; Arias, C.; Cabot, P.L. Structure and electrocatalytic performance of carbon-supported platinum nanoparticles. *J. Power Sources* **2009**, *190*, 201–209. [CrossRef]
57. Rizo, R.; Sebastián, D.; Lázaro, M.J.; Pastor, E. On the design of Pt-Sn efficient catalyst for carbon monoxide and ethanol oxidation in acid and alkaline media. *Appl. Catal. B Environ.* **2017**, *200*, 246–254. [CrossRef]
58. Powder Diffraction File (2018). International Centre for Diffraction Data (ICDD). 12 Campus Boulevard. Newton Square, PA, USA. 2018. Available online: http://www.icdd.com (accessed on 30 March 2020).
59. Hosseini, M.G.; Mahmoodi, R. Preparation method of Ni@Pt/C nanocatalyst affects the performance of direct borohydride-hydrogen peroxide fuel cell: Improved power density and increased catalytic oxidation of borohydride. *J. Colloid Interface Sci.* **2017**, *500*, 264–275. [CrossRef]
60. Maya-Cornejo, J.; Carrera-Cerritos, R.; Sebastián, D.; Ledesma-García, J.; Arriaga, L.G.; Aricò, A.S.; Baglio, V. PtCu catalyst for the electro-oxidation of ethanol in an alkaline direct alcohol fuel cell. *Int. J. Hydrogen Energy* **2017**, *42*, 27919–27928. [CrossRef]
61. Velázquez-Palenzuela, A.; Centellas, F.; Garrido, J.A.; Arias, C.; Rodríguez, R.M.; Brillas, E.; Cabot, P.L. Structural characterization of Ru-modified carbon-supported Pt nanoparticles using spontaneous deposition with CO oxidation activity. *J. Phys. Chem. C* **2012**, *116*, 18469–18478. [CrossRef]
62. Sugimoto, W.; Yokoshima, K.; Murakami, Y.; Takasu, Y. Charge storage mechanism of nanostructured anhydrous and hydrous ruthenium-based oxides. *Electrochim. Acta* **2006**, *52*, 1742–1748. [CrossRef]
63. Dos Santos, L.; Colmati, F.; González, E.R. Preparation and characterization of supported Pt-Ru catalysts with a high Ru content. *J. Power Sources* **2006**, *159*, 869–877. [CrossRef]
64. Wang, H.; Baltruschat, H. DEMS Study on Methanol Oxidation at Poly- and Monocrystalline Platinum Electrodes: The Effect of Anion, Temperature, Surface Structure, Ru Adatom, and Potential. *J. Phys. Chem.* **2007**, *111*, 7038–7048. [CrossRef]

65. Velázquez-Palenzuela, A.; Centellas, F.; Garrido, J.A.; Arias, C.; Rodríguez, R.M.; Brillas, E.; Cabot, P.L. Kinetic analysis of carbon monoxide and methanol oxidation on high performance carbon-supported Pt-Ru electrocatalyst for direct methanol fuel cells. *J. Power Sources* **2011**, *196*, 3503–3512. [CrossRef]
66. Antolini, E. Carbon supports for low-temperature fuel cell catalysts. *Appl. Catal. B Environ.* **2009**, *88*, 1–24. [CrossRef]
67. Velázquez-Palenzuela, A.; Brillas, E.; Arias, C.; Centellas, F.; Garrido, J.A.; Rodríguez, R.M.; Cabot, P.L. Structural analysis of carbon-supported Ru-decorated Pt nanoparticles synthesized using forced deposition and catalytic performance towards CO, methanol, and ethanol electro-oxidation. *J. Catal.* **2013**, *298*, 112–121. [CrossRef]